

Collective spin mode in a multi-component system of coupled itinerant and localized electrons

Fan Yang,¹ Su-Peng Kou,² and Zheng-Yu Weng^{3,*}

¹*Department of Physics, Beijing Institute of Technology, Beijing 100081, P.R.China*

²*Department of Physics, Beijing Normal University, Beijing, 100875, P.R.China*

³*Institute for Advanced Study, Tsinghua University, Beijing, 100084, P.R.China*

(Dated: November 3, 2018)

We study collective spin excitations of a magnetically ordered state in a multi-component system composed of both itinerant electrons and local moments. Here the induced spin-density-wave (SDW) ordering of itinerant electrons and the collinear antiferromagnetic (AF) ordering of local moments are locked together via a Hund's rule coupling. We show that the Goldstone theorem still holds at the RPA level with the gapless spin wave protected inside the small SDW gap of itinerant electrons, which, however, is fragile in the presence of ion-anisotropy. A gapped "out-of-phase" spin mode extending over a much wider energy scale above the SDW gap is found to be more robust against the ion-anisotropy, which is mainly contributed by the local moment fluctuations. While the scattering between the Goldstone mode and itinerant electrons diminishes within the SDW gap, the "out-of-phase" mode will strongly interact with itinerant electrons and thus dominate the spin and charge dynamics in such an ordered phase. Possible relevance of such a model to the iron-pnictides will be also discussed.

I. INTRODUCTION

The recent discovery of high- T_c superconductors in the iron pnictides¹ has renewed a tremendous interest in the interplay between the magnetism and superconductivity. The similar issue has been vigorously investigated in the high- T_c cuprates over two decades, where antiferromagnetism has been firmly related to the localized electrons of the Mott insulator in undoped cuprate compounds². By contrast, in the pnictides, the undoped parent material is not a simple Mott-Hubbard insulator but resembles a multi-band bad metal - i.e., the iron

3d-electrons are believed to be quite itinerant with their hybridized multi-orbitals forming multiple Fermi pockets at the Fermi level³⁻⁷.

It is natural for many to consider the spin-density-wave (SDW) order, observed in the undoped parent compounds by the neutron scattering measurements⁸, as originated from the same itinerant electrons via Fermi surface nesting³. This picture seems more consistent in explaining the ARPES⁹⁻¹¹, transport^{1,12}, and optical properties¹³ than a purely localized model, e.g., the J_1 - J_2 model¹⁴⁻¹⁷, where a Mott-insulator transition has been implied. The latter is more reasonable in explaining the spin excitations in neutron scattering¹⁷ and high-temperature magnetic susceptibility¹⁸⁻²⁰, but obviously fails in understanding the bad metal behavior^{1,13,21,22} and the presence of the small Fermi pockets^{9-11,23,24} in the parent compounds.

Based on the overall experimental evidence, an alternative picture has been recently proposed²⁵, which assumes that some kind of orbital-selective Mott transition happens in the iron 3d orbitals of the pnictides such that both itinerant and Mott-localized electron coexist in the system. The minimal model²⁵ based on this picture tries to reconcile the seemingly contradictory experimental facts and provides a natural understanding of the unified driving force behind the collinear antiferromagnetic (AF) order and high-temperature superconductivity. Recently a microscopic realization of an orbital-selective Mott transition in the pnictides has been studied^{26,27} based on the dynamic mean-field theory, which lends further support to this model.

The key and unique feature for such a coexistent itinerant and localized electron system is that the two subsystems share the *same* characteristic momenta at $\mathbf{Q}_s = (\pi, 0)$ or $(0, \pi)$. Namely, the hole and electron Fermi surface pockets around Γ and M points in the Brillouin zone (BZ) are approximately connected by \mathbf{Q}_s in the undoped case (i.e., close to the Fermi surface nesting), and at the same time, the local moments are strongly correlated at the AF wavevectors \mathbf{Q}_s . As a consequence, the local Hund's rule coupling between the itinerant electrons and local moments can be significantly enhanced around \mathbf{Q}_s , which is called the “*resonant effect*”²⁵. At low temperature, such a “resonant effect” can serve as a predominant force in driving the *magnetic* or *pairing instability* at different dopings. Here the magnetic phase is predicted²⁵ to be an induced SDW order of the itinerant electrons locking with the collinear AF order of the local moments at the *same* \mathbf{Q}_s . Corresponding to such an AF ordering, a small SDW gap will open up in the excitation spectrum of itinerant electrons,

although *not* necessarily pinned at the Fermi level as in an SDW state purely driven by Fermi surface nesting. At the mean-field level, the low-lying AF fluctuation of the local moments is also gapped at \mathbf{Q}_s due to the mutual locking of the magnetic orders in the two subsystems. Therefore, after the spontaneous magnetic symmetry breaking, the strong “resonant” scattering between the two degrees of freedom gets substantially reduced, which leads to a very coherent charge transport contributed by the ungapped part of the Fermi surfaces in consistency with the optical measurement¹³.

However, it remains an important issue whether a gapless spin wave, i.e., a Goldstone mode, is still present in the magnetically ordered state of such a multi-component system. To answer this question, one has to go beyond the mean-field theory to study the collective spin fluctuations, which is also important in order to self-consistently address the issue how the charge dynamics gets reshaped in the AF phase. In this paper, we shall address this issue with using a realistic five-band model⁷ to characterize the itinerant electrons near the Fermi pockets, and a J_1 - J_2 type model to describe the Mott-localized electrons. Then we study the Hund’s rule coupling between the itinerant and localized electrons at the RPA level in the magnetic ordered phase. We demonstrate that the Goldstone theorem indeed holds at the RPA level as a gapless spin wave emerges within the mean-field SDW gap of itinerant electrons. But it is fragile against the ion-anisotropy. We further find that the coupling between the Goldstone mode and the charge carriers diminishes in the long-wavelength around \mathbf{Q}_s as expected. On the other hand, distinct from a single component system, a gapped “out-of-phase” collective spin mode is also present with its high-energy part predominantly contributed by the local moments whose energy scale $\sim J_2$ extends over a much wider regime than the SDW gap. Its low-energy part gets strongly renormalized by coupling to the itinerant electrons around \mathbf{Q}_s —it becomes gapped once the mean-field SDW order forms by itinerant electrons, which is not significantly modified at the RPA level. Furthermore, such an “out-of-phase” mode is not sensitive to a weak ion-anisotropy effect and is thus more robust than the Goldstone mode. The existence of the two branches of spin excitations in the AF state is a unique prediction of the present multi-component model. In particular, it is this “out-of-phase” spin mode that remains strongly interacting with itinerant electrons, at an energy higher than its gap, and therefore dominates the high-energy magnetic and transport properties in the magnetically ordered phase.

The remainder of the paper is organized as follows. In Sec. II, we introduce the model

and present the mean-field treatment in the magnetically ordered state. Then in Sec. III, we discuss the spin dynamics at the RPA level and demonstrate that the spin collective excitations are split into a gapless Goldstone mode which is upper-bounded and a gapped out-of-phase mode which extends over a much wider energy scale. In Sec. IV, we study the scattering between the collective spin modes and the itinerant electrons based on the single-particle self-energy of the itinerant electrons and the optical conductivity, which illustrate that the out-of-phase mode will play a dominant role beyond its energy gap. Finally, Sec. V is devoted to the discussion and conclusion.

II. A MULTI-COMPONENT SYSTEM OF COUPLED ITINERANT AND LOCALIZED ELECTRONS

A. Model

We consider a multi-component system composed of coexistent multiband itinerant and Mott-localized electrons described by

$$H = H_{\text{it}} + H_{\text{lo}} + H_{J_H}. \quad (1)$$

Here H_{it} is a tight-binding model of multiband itinerant electrons:

$$H_{\text{it}} = - \sum_{i,j,m,n,\sigma} t_{ij,mn} c_{im\sigma}^\dagger c_{jn\sigma}, \quad (2)$$

where m and n are the orbital indices. The hopping integral $t_{ij,mn}$ in H_{it} will be given based on a realistic five-band tight-binding model proposed⁷ to describe the undoped iron-pnictide materials. The resulting band structure near the Fermi energy is shown in Fig. 1 by the solid (black) curves, with the Fermi surface shown in Fig. 2(a) in the undoped case (i.e., six electrons per site). Note that some slight modification with a global renormalization factor reducing the bandwidth has been phenomenologically made here in order to be consistent with ARPES^{9–11,24}. As shown in Fig. 2(a), the itinerant electrons form hole and electron pockets at the Fermi energy, which are located at the Γ point and the M point, respectively, separated by the momenta \mathbf{Q}_s in an extended BZ.

The second term H_{lo} in (1) describes the localized electrons in which a Mott gap is opened up via the so-called orbital-selective Mott transition²⁵. Namely, the corresponding

electrons only contribute to spin fluctuations, near the Fermi energy, by the local moments formed from the filled lower Hubbard band. Note that a microscopic realization of the orbital-selective Mott transition in such a system has been recently discussed based on the dynamic mean-field theory^{26,27}. We shall simply use a J_1 - J_2 model of $S = 1$ to depict the superexchange couplings between these local moments, i.e.,

$$H_{\text{lo}} = J_1 \sum_{\langle ij \rangle} \hat{\mathbf{S}}_i \cdot \hat{\mathbf{S}}_j + J_2 \sum_{\langle\langle ij \rangle\rangle} \hat{\mathbf{S}}_i \cdot \hat{\mathbf{S}}_j \quad (3)$$

where $\langle ij \rangle$ and $\langle\langle ij \rangle\rangle$ denote the nearest-neighbor and next-nearest-neighbor coupling, respectively. Here we assume $J_1 < 2J_2$ such that the ground state of H_{lo} itself may form a collinear AF ordering at the wavevector \mathbf{Q}_s . In principle, the same five-band electrons in iron-pnictides should contribute to both itinerant and local moment degrees of freedom. But for simplicity we treat H_{it} and H_{lo} as if they govern *independent* degrees of freedom in the low-energy sector near the Fermi energy, so long as the Mott gap remains a large energy scale. We ignore the issues like how the Fermi surface shape gets affected by the orbital-selective Mott transition as well as how the Luttinger volume is correctly accounted for and mainly focus on the low-energy physics in the present work.

The third term H_{J_H} in (1) is the Hund's rule coupling between the spins of itinerant and the localized electrons:

$$H_{J_H} = - \sum_{i,m} J_0^m \hat{\mathbf{S}}_i \cdot \hat{\mathbf{s}}_{im}. \quad (4)$$

where $\hat{\mathbf{s}}_{im} = c_{im}^\dagger \hat{\sigma} c_{im}$ is the spin operator of the itinerant electrons in the m -th orbital and $\hat{\mathbf{S}}_i$ denotes the localized moment at site i . J_0^m is a renormalized Hund's rule coupling constant. For simplicity, we shall assume a single $J_0^m = J_0$ for different orbitals throughout the paper.

Originally a simpler form of (1) was proposed as a minimal model to describe the low-energy physics in the iron-pnictides²⁵. The most important feature in such a model Hamiltonian is that the peculiar momenta \mathbf{Q}_s , which on the one hand connects the two Fermi pockets of the itinerant electrons at Γ and M points, respectively, and on the other hand coincide with the AF wavevectors of the local moments. It implies *strongly enhanced* dynamic coupling between the itinerant and local moment degrees of freedom, once the short-range AF correlations of the local moments set in around \mathbf{Q}_s even in a high-temperature normal state. With the decrease of temperature, such a ‘‘resonant’’ coupling will result in an AF

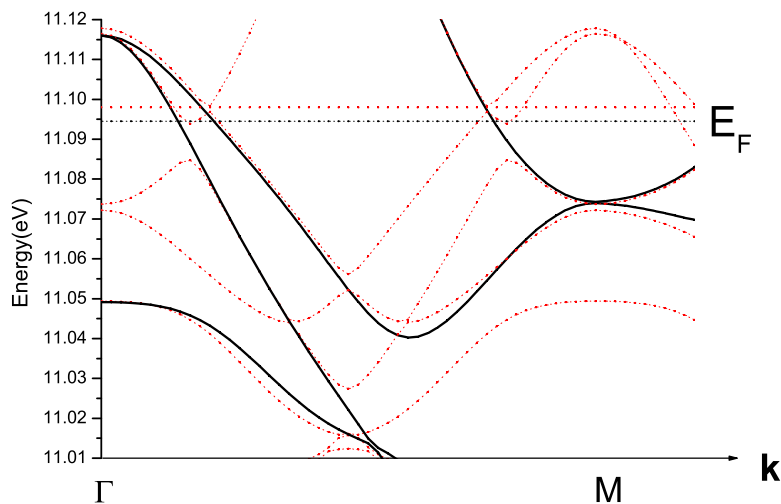


FIG. 1: (Color online) The band structure near the Fermi energy for the five-band model described by H_{it} in (2) (black solid curves) in the undoped case. The reconstruction of the band structure of itinerant electrons in the presence of a collinear AF order is shown by red dotted curves.

ordered phase with distinctive dynamic behaviors to be explored below, as compared to an ordinary SDW state of a pure itinerant electron system due to the Fermi-surface nesting mechanism or the collinear AF state of a pure J_1 - J_2 mode.

B. Mean-field treatment in the collinear AF ordered state

In the following we first use a mean-field approximation to study the collinear AF ordered state in (1). The spin and charge dynamics at the RPA level will be investigated in the later sections.

We start with the interaction term H_{J_H} in (4) between the two sub-systems. By introducing two order parameters of magnetization for the local-moments, $M_{(lo)}$, and itinerant-electrons, $M_{(it)}$, respectively, as in $\langle \hat{S}_i^z \rangle \equiv M_{(lo)} e^{i\mathbf{Q}_s \cdot \mathbf{r}_i}$ and $\sum_m \langle \hat{s}_{im}^z \rangle \equiv M_{(it)} e^{i\mathbf{Q}_s \cdot \mathbf{r}_i}$, one obtains the following linearization in H_{J_H} , given by

$$\begin{aligned}
 H_{J_H} &\rightarrow H_I = -J_0 \sum_i \left[M_{(lo)} e^{i\mathbf{Q}_s \cdot \mathbf{r}_i} \sum_m s_{im}^z + M_{(it)} e^{i\mathbf{Q}_s \cdot \mathbf{r}_i} \hat{S}_i^z \right] \\
 &\equiv H_{I(it)} + H_{I(lo)}.
 \end{aligned} \tag{5}$$

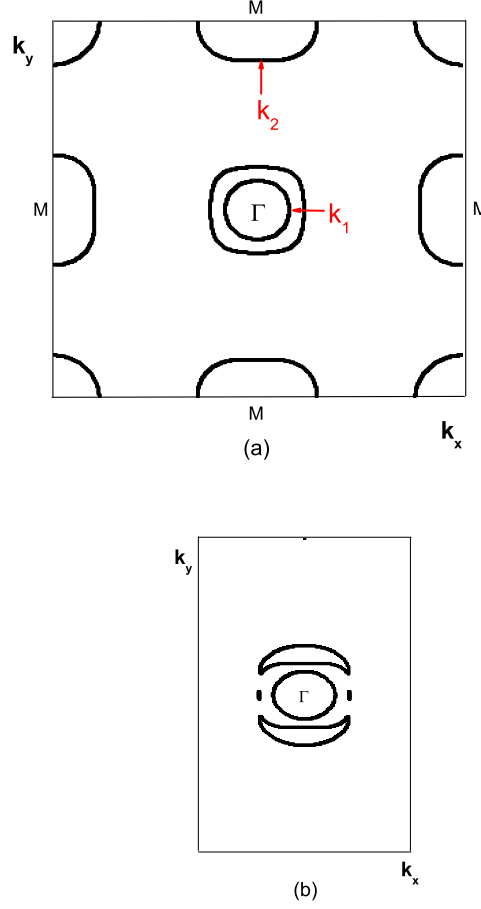


FIG. 2: (Color online) (a): The Fermi pockets of the itinerant electrons in the undoped case. (b): The reconstruction of the Fermi surface in the presence of a collinear AF order with a wavevector $\mathbf{Q}_s = (\pi, 0)$ in the reduced BZ.

Below the effect of such mean-field terms on the local moments and itinerant electrons will be explored in a self-consistent way.

1. Local moment part

In the magnetic order phase with $\langle \hat{S}_i^z \rangle = M_{(\text{lo})} e^{i\mathbf{Q}_s \cdot \mathbf{r}_i}$, one may first use the conventional spin-wave approximation to treat H_{lo} in (3) and then add $H_{I(\text{lo})}$ in (5) to incorporate the effect of the coupling to the itinerant electrons. Here \mathbf{Q}_s is chosen to be $(\pi, 0)$.

Introduce the Holstein-Primakoff (HP) transformation

$$\begin{aligned}\hat{S}_{iA}^+ &= \sqrt{2S - a_i^\dagger a_i a_i}, \quad \hat{S}_{iA}^- = a_i^\dagger \sqrt{2S - a_i^\dagger a_i}, \quad \hat{S}_{iA}^z = S - a_i^\dagger a_i, \\ \hat{S}_{jB}^+ &= \sqrt{2S - b_j^\dagger b_j b_j}, \quad \hat{S}_{jB}^- = b_j \sqrt{2S - b_j^\dagger b_j}, \quad \hat{S}_{jB}^z = -S + b_j^\dagger b_j,\end{aligned}\quad (6)$$

where A and B sublattices are defined by the staggered factor $e^{i\mathbf{Q}_s \cdot \mathbf{r}_i} = \pm 1$. Under the approximation $\sqrt{2S - a_i^\dagger a_i} \approx \sqrt{2S - b_i^\dagger b_i} \approx \sqrt{2S}$ and using the boson operators in the momentum space

$$a_i = \left(\frac{2}{N}\right)^{1/2} \sum_{\mathbf{k}}' a_{\mathbf{k}} \exp(i\mathbf{k} \cdot \mathbf{r}_i), \quad (7)$$

$$b_j = \left(\frac{2}{N}\right)^{1/2} \sum_{\mathbf{k}}' b_{\mathbf{k}} \exp(i\mathbf{k} \cdot \mathbf{r}_j), \quad (8)$$

H_{10} is transformed into

$$H_{10} = S \sum_{\mathbf{k}}' [\Gamma_{\mathbf{k}}(a_{\mathbf{k}}^\dagger a_{\mathbf{k}} + b_{\mathbf{k}}^\dagger b_{\mathbf{k}}) + M_{\mathbf{k}}(a_{\mathbf{k}} b_{-\mathbf{k}} + a_{\mathbf{k}}^\dagger b_{-\mathbf{k}}^\dagger)], \quad (9)$$

where $\sum_{\mathbf{k}}'$ means that the sum is within a reduced BZ with

$$\Gamma_{\mathbf{k}} = 4J_2 + 2J_1 \cos k_y, \quad (10)$$

$$M_{\mathbf{k}} = 2J_1 \cos k_x + 4J_2 \cos k_x \cdot \cos k_y. \quad (11)$$

Then (9) can be diagonalized by the Bogolubov transformation

$$\begin{aligned}a_{\mathbf{k}} &= u_{\mathbf{k}} \alpha_{\mathbf{k}} + v_{\mathbf{k}} \beta_{-\mathbf{k}}^\dagger \\ b_{-\mathbf{k}}^\dagger &= v_{\mathbf{k}} \alpha_{\mathbf{k}} + u_{\mathbf{k}} \beta_{-\mathbf{k}}^\dagger,\end{aligned}\quad (12)$$

as follows

$$H_{10} = \sum_{\mathbf{k}}' \omega_{\mathbf{k}} (\alpha_{\mathbf{k}}^\dagger \alpha_{\mathbf{k}} + \beta_{\mathbf{k}}^\dagger \beta_{\mathbf{k}}), \quad (13)$$

where

$$u_{\mathbf{k}} = \left(\frac{\omega_{\mathbf{k}} + \Gamma_{\mathbf{k}}}{2\omega_{\mathbf{k}}}\right)^{\frac{1}{2}}, \quad (14)$$

$$v_{\mathbf{k}} = -\left(\frac{-\omega_{\mathbf{k}} + \Gamma_{\mathbf{k}}}{2\omega_{\mathbf{k}}}\right)^{\frac{1}{2}} \text{sgn}(M_{\mathbf{k}}), \quad (15)$$

$$\omega_{\mathbf{k}} = S \sqrt{\Gamma_{\mathbf{k}}^2 - M_{\mathbf{k}}^2}, \quad (16)$$

Here $\omega_{\mathbf{k}}$ is gapless at $\mathbf{k} = \mathbf{Q}_s$ as the Goldstone mode of H_{10} in the AF ordered phase.

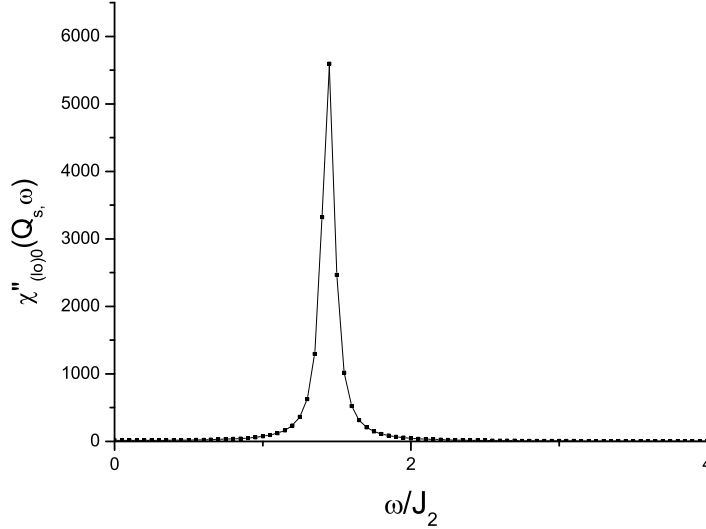


FIG. 3: (Color online) Dynamic spin susceptibility of local-moments at mean-field level, i.e. $\chi''_{(lo)0\mathbf{q}}(\omega) \equiv -2\text{Im}\chi_{(lo)0}^{+-}(\mathbf{q}, \mathbf{q}, \omega)$ at $\mathbf{q} = \mathbf{Q}_s$ shows a gap, given by (19), which is opened up in the presence of a mean-field coupling to the SDW ordering of itinerant electrons, with the parameters given in Sec. IIB.

Now let us add $H_{I(lo)}$ in (5) arising from the mean-field decoupling of H_{J_H} . It can be reexpressed in the spin-wave formalism by

$$H_{I(lo)} = J_0 M_{(it)} \sum_{\mathbf{k}}' \left(a_{\mathbf{k}}^\dagger a_{\mathbf{k}} + b_{\mathbf{k}}^\dagger b_{\mathbf{k}} \right) + \text{const.} \quad (17)$$

This term will lead to a shift in $\Gamma_{\mathbf{k}}$ defined in (10): i.e., $\Gamma_{\mathbf{k}} \rightarrow \Gamma_{\mathbf{k}} + J_0 M_{(it)}/S$. As a result, the dispersion of the spin wave is modified by

$$\omega_{\mathbf{k}} \rightarrow \omega_{\mathbf{k}} = S \sqrt{(\Gamma_{\mathbf{k}} + J_0 M_{(it)}/S)^2 - M_{\mathbf{k}}^2}. \quad (18)$$

In particular, $\omega_{\mathbf{k}}$ is no longer gapless at \mathbf{Q}_s with an energy gap induced by $M_{(it)}$ as

$$\omega_{\mathbf{Q}_s} = \sqrt{4M_{(it)}S J_0 (2J_2 + J_1) + (M_{(it)}J_0)^2}. \quad (19)$$

The order parameter $M_{(lo)}$ can be self-consistently calculated as

$$\begin{aligned} M_{(lo)} &= S - \frac{1}{N} \left\langle \sum_{\mathbf{k}}' \left(a_{\mathbf{k}}^\dagger a_{\mathbf{k}} + b_{\mathbf{k}}^\dagger b_{\mathbf{k}} \right) \right\rangle \\ &= S - \frac{2}{N} \sum_{\mathbf{k}}' v_{\mathbf{k}}^2, \end{aligned} \quad (20)$$

where $v_{\mathbf{k}}$ is defined by (15) with $\Gamma_{\mathbf{k}} \rightarrow \Gamma_{\mathbf{k}} + J_0 M_{(\text{it})}/S$ and $\omega_{\mathbf{k}}$ defined in (18).

Finally, the spin-spin correlations for the local-moment defined by

$$\chi_{(\text{lo})}^{+-}(\mathbf{q}, \mathbf{q}, t) = -i \left\langle T \hat{S}_{\mathbf{q}}^+(t) \hat{S}_{-\mathbf{q}}^-(0) \right\rangle, \quad \chi_{(\text{lo})}^{+-}(\mathbf{q}, \mathbf{q} + \mathbf{Q}_s, t) = -i \left\langle T \hat{S}_{\mathbf{q}}^+(t) \hat{S}_{-\mathbf{q}-\mathbf{Q}_s}^-(0) \right\rangle,$$

can be obtained for this mean-field spin-wave state in the frequency space as

$$\begin{aligned} \chi_{(\text{lo})0}^{+-}(\mathbf{q}, \mathbf{q}, \omega) &= M_{(\text{lo})} (u_{\mathbf{k}} + v_{\mathbf{k}})^2 \left(\frac{1}{\omega - \omega_{\mathbf{k}} + i0^+} + \frac{1}{-\omega - \omega_{\mathbf{k}} + i0^+} \right), \\ \chi_{(\text{lo})0}^{+-}(\mathbf{q}, \mathbf{q} + \mathbf{Q}_s, \omega) &= M_{(\text{lo})} \left(\frac{1}{\omega - \omega_{\mathbf{k}} + i0^+} - \frac{1}{-\omega - \omega_{\mathbf{k}} + i0^+} \right), \end{aligned} \quad (21)$$

The spin gap in (19) is clearly illustrated in the dynamic spin susceptibility $\chi_{(\text{lo})0\mathbf{q}}''(\omega) \equiv -2\text{Im}\chi_{(\text{lo})0}^{+-}(\mathbf{q}, \mathbf{q}, \omega)$ at $\mathbf{q} = \mathbf{Q}_s$ as shown in Fig. 3 (the parameters used are to be given below). It is pointed out that in the above calculation, we have further used the approximation: $S_{iA(B)}^+ \rightarrow \sqrt{2M_{(\text{lo})}} a_i^\dagger \left(\sqrt{2M_{(\text{lo})}} b_i^\dagger \right)$ in the original HP transformation (6) such that the spin commutation relations are satisfied at the mean-field level, i.e. $\langle \hat{\mathbf{S}} \times \hat{\mathbf{S}} \rangle = i\hbar \langle \hat{\mathbf{S}} \rangle$.

2. Itinerant electron part

Combining $H_{I(\text{it})}$ in (5) with the band kinetics energy term H_{it} in (2), the mean-field Hamiltonian of the itinerant-electrons reads

$$\begin{aligned} H_{\text{it}} + H_{I(\text{it})} &= \sum'_{\mathbf{k}mn\sigma} \left[f_{mn}(\mathbf{k}) c_{\mathbf{k}m\sigma}^+ c_{\mathbf{k}n\sigma} + f_{mn}(\mathbf{k} + \mathbf{Q}_s) c_{\mathbf{k}+\mathbf{Q}_s,m\sigma}^\dagger c_{\mathbf{k}+\mathbf{Q}_s,n\sigma} \right. \\ &\quad \left. - \frac{J_0 M_{(\text{lo})} \sigma}{2} \delta_{mn} \left(c_{\mathbf{k}+\mathbf{Q}_s,m\sigma}^\dagger c_{\mathbf{k},n\sigma} + c_{\mathbf{k},m\sigma}^\dagger c_{\mathbf{k}+\mathbf{Q}_s,n\sigma} \right) \right] \\ &\equiv \sum'_{\mathbf{k}\sigma} X_{\mathbf{k}\sigma}^\dagger H_\sigma X_{\mathbf{k}\sigma}, \end{aligned} \quad (22)$$

where

$$f_{mn}(\mathbf{k}) = 2 \sum_{\mathbf{r}_i - \mathbf{r}_j} t_{ij,mn} e^{i\mathbf{k} \cdot (\mathbf{r}_i - \mathbf{r}_j)}. \quad (23)$$

In the second line of (22), the 10×10 matrix H_σ for the five bands is defined by

$$(H)_\sigma = \begin{pmatrix} F_{\mathbf{k}} & -\gamma I \sigma \\ -\gamma I \sigma & F_{\mathbf{k}+\mathbf{Q}_s} \end{pmatrix}, \quad (24)$$

with

$$\gamma = \frac{J_0 M_{(\text{lo})}}{2}. \quad (25)$$

Here I is the 5×5 identity matrix and F is the matrix defined by $(F)_{m,n} = f_{mn}$. The column vector $X_{\mathbf{k}\sigma}$ is given by

$$X_{\mathbf{k}\sigma}^T \equiv (c_{\mathbf{k},1\sigma}, c_{\mathbf{k},2\sigma} \cdots c_{\mathbf{k}+\mathbf{Q}_s,1\sigma} c_{\mathbf{k}+\mathbf{Q}_s,2\sigma} \cdots). \quad (26)$$

By diagonalizing the 10×10 matrix $(H)_\sigma$

$$U_\sigma^\dagger H_\sigma U_\sigma = D, \quad (27)$$

one gets

$$H_{\text{it}} + H_{I(\text{it})} = \sum'_{\mathbf{k}\alpha\sigma} E_{\mathbf{k}\alpha} c_{\mathbf{k}\alpha\sigma}^\dagger c_{\mathbf{k}\alpha\sigma}, \quad (28)$$

where the band energy $E_{\mathbf{k}\alpha}$ is equal to the α -th diagonal element of D , presented in Fig. 1 by the red dotted curves with the corresponding Fermi surface in the reduced BZ shown in Fig. 2(b) in the undoped case. Here the order parameter $M_{(\text{it})}$ is self-consistently determined by

$$\begin{aligned} M_{(\text{it})} &= \frac{1}{2N} \sum_{in} e^{i\mathbf{Q}_s \cdot \mathbf{r}_i} \langle c_{in\uparrow}^\dagger c_{in\uparrow} - c_{in\downarrow}^\dagger c_{in\downarrow} \rangle \\ &= \frac{2}{N} \sum'_{E_{\mathbf{k}\alpha} < E_F} \sum_n U_{\mathbf{k}\uparrow}^*(n+5, \alpha) U_{\mathbf{k}\uparrow}(n, \alpha). \end{aligned} \quad (29)$$

Together with (20), we find $M_{(\text{it})} = 0.252$ and $M_{(\text{lo})} = 0.892$ by choosing $J_0 = 20$ meV at $J_1 = 0$, and $J_2 = 20$ meV for $S = 1$. In the following we shall use these parameters to examine various spin and charge dynamics (we have also checked other small ratios of J_1/J_2 and found the results remain qualitatively unchanged).

Similar mean-field results have been previously obtained²⁵ in a simpler model of (1), where a spin gap similar to (19) is also found in the spin-wave spectrum of local moments due to the Hund's rule coupling to the SDW order of the itinerant electrons. Such a gap will protect the collinear AF ordering jointly formed by *both* local moments and itinerant electrons below a transition temperature T_{SDW} . For example, the presence of this gap is reflected by a step reduction of the uniform spin susceptibility below T_{SDW} , which is consistent²⁵ with the experimental measurement in the iron-pnictides^{18,19}. However, according to the Goldstone theorem, a gapless mode is generally expected to exist in the AF ordered state. How such a Goldstone mode can be reconciled with the gapped local moment fluctuations discussed above will be studied at the RPA level in the next section.

Finally, the spin-spin correlation functions of itinerant electrons are defined as

$$\chi_{(\text{it})}^{+-}(\mathbf{q}, \mathbf{q}, t) = -i \langle T \hat{s}_{\mathbf{q}}^+(t) \hat{s}_{-\mathbf{q}}^-(0) \rangle, \quad \chi_{(\text{it})}^{+-}(\mathbf{q}, \mathbf{q} + \mathbf{Q}_s, t) = -i \langle T \hat{s}_{\mathbf{q}}^+(t) \hat{s}_{-\mathbf{q}-\mathbf{Q}_s}^-(0) \rangle,$$

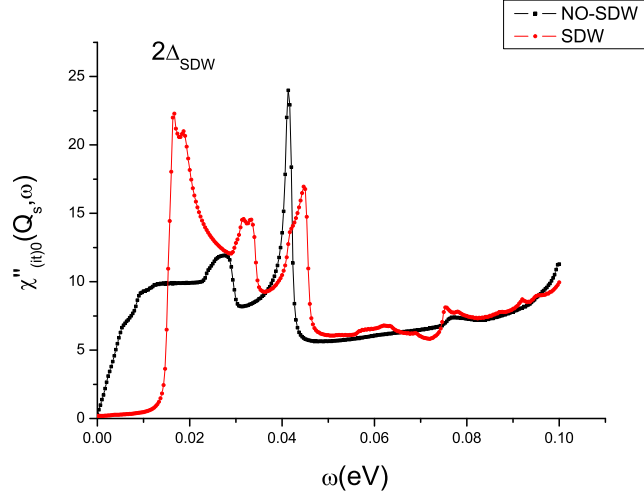


FIG. 4: (Color online) Dynamic spin susceptibility of itinerant electrons at the mean-field level, i.e. $\chi''_{(it)0\mathbf{Q}_s}(\omega) \equiv -2\text{Im}\chi_{(it)0}^{+-}(\mathbf{Q}_s, \mathbf{Q}_s, \omega)$ with and without SDW order. A gap $2\Delta_{\text{SDW}}$ in the SDW ordered case is clearly shown.

where $\hat{s}_{\mathbf{q}}^{\pm}$ is the sum over all the five-orbital

$$\hat{s}_{\mathbf{q}}^{\pm} = \sum_m \hat{s}_{\mathbf{q}m}^{\pm}. \quad (30)$$

In the above mean-field state, after a straightforward but tedious calculation one obtains, for example,

$$\begin{aligned} \chi_{(it)0}^{+-}(\mathbf{q}, \mathbf{q}, \omega) = & \sum_{\mathbf{k} \in R, \mathbf{k}+\mathbf{q} \in R, E_{\mathbf{k},\alpha} > E_F, E_{\mathbf{k}+\mathbf{q},\beta} < E_F} \frac{|V_{\mathbf{k},\mathbf{k}+\mathbf{q}}^{(1)}(\alpha, \beta)|^2}{\omega - (E_{\mathbf{k},\alpha} - E_{\mathbf{k}+\mathbf{q},\beta}) + i0^+} \\ & + \sum_{\mathbf{k} \in R, \mathbf{k}+\mathbf{q} \notin R, E_{\mathbf{k},\alpha} > E_F, E_{\mathbf{k}+\mathbf{q} \pm \mathbf{Q}_s, \beta} < E_F} \frac{|V_{\mathbf{k},\mathbf{k}+\mathbf{q} \pm \mathbf{Q}_s}^{(2)}(\alpha, \beta)|^2}{\omega - (E_{\mathbf{k},\alpha} - E_{\mathbf{k}+\mathbf{q} \pm \mathbf{Q}_s, \beta}) + i0^+} \\ & + \sum_{\mathbf{k} \in R, \mathbf{k}-\mathbf{q} \in R, E_{\mathbf{k},\alpha} > E_F, E_{\mathbf{k}-\mathbf{q},\beta} < E_F} \frac{|V_{\mathbf{k}-\mathbf{q},\mathbf{k}}^{(1)}(\beta, \alpha)|^2}{-\omega - (E_{\mathbf{k},\alpha} - E_{\mathbf{k}-\mathbf{q},\beta}) + i0^+} \\ & + \sum_{\mathbf{k} \in R, \mathbf{k}-\mathbf{q} \notin R, E_{\mathbf{k},\alpha} > E_F, E_{\mathbf{k}-\mathbf{q} \pm \mathbf{Q}_s, \beta} < E_F} \frac{|V_{\mathbf{k}-\mathbf{q} \pm \mathbf{Q}_s, \mathbf{k}}^{(2)}(\beta, \alpha)|^2}{-\omega - (E_{\mathbf{k},\alpha} - E_{\mathbf{k}-\mathbf{q} \pm \mathbf{Q}_s, \beta}) + i0^+}, \quad (31) \end{aligned}$$

for the momentum \mathbf{q} within the reduced BZ, i.e. $\mathbf{q} \in R$, and

$$\begin{aligned} V_{\mathbf{k},\mathbf{q}}^{(1)}(\alpha, \beta) &\equiv \sum_m [U_{\mathbf{k}\downarrow}^*(m, \alpha) U_{\mathbf{q}\uparrow}(m, \beta) + U_{\mathbf{k}\downarrow}^*(m+5, \alpha) U_{\mathbf{q}\uparrow}(m+5, \beta)] \\ V_{\mathbf{k},\mathbf{q}}^{(2)}(\alpha, \beta) &\equiv \sum_m [U_{\mathbf{k}\downarrow}^*(m, \alpha) U_{\mathbf{q}\uparrow}(m+5, \beta) + U_{\mathbf{k}\downarrow}^*(m+5, \alpha) U_{\mathbf{q}\uparrow}(m, \beta)], \end{aligned} \quad (32)$$

with, say,

$$\hat{s}_{-\mathbf{q}}^- = \sum_{\alpha\beta, \mathbf{k} \in R, \mathbf{k}+\mathbf{q} \in R} c_{\mathbf{k},\alpha,\downarrow}^\dagger c_{\mathbf{k}+\mathbf{q},\beta\uparrow} V_{\mathbf{k},\mathbf{k}+\mathbf{q}}^{(1)}(\alpha, \beta) + \sum_{\alpha\beta, \mathbf{k} \in R, \mathbf{k}+\mathbf{q} \notin R} c_{\mathbf{k},\alpha,\downarrow}^\dagger c_{\mathbf{k}+\mathbf{q}\pm\mathbf{Q}_s,\beta\uparrow} V_{\mathbf{k},\mathbf{k}+\mathbf{q}\pm\mathbf{Q}_s}^{(2)}(\alpha, \beta). \quad (33)$$

The other Green's function can be similarly obtained. Numerical calculation for the dynamic spin susceptibility of the itinerant-electrons at the mean-field level, i.e. $\chi''_{(\text{it})0\mathbf{Q}_s}(\omega) \equiv -2\text{Im}\chi_{(\text{it})0}^{+-}(\mathbf{Q}_s, \mathbf{Q}_s, \omega)$ is presented in Fig. 4 with and without SDW order, where the suppressing of the low-frequency spectrum by the SDW gap at $2\Delta_{\text{SDW}}$ is clearly shown.

III. SPIN DYNAMICS

In this section, we shall calculate the dynamic spin susceptibility at the RPA level beyond the above mean-field approximation, by which both a Goldstone mode and a gapped collective spin mode in the AF ordered phase can be recovered.

A. RPA treatment

The Hund's rule interaction between the local moments and itinerant electrons in (4) is rewritten as

$$H_{J_H} = -J_0 \sum_{\mathbf{q}} \hat{\mathbf{S}}_{\mathbf{q}} \cdot \hat{\mathbf{s}}_{-\mathbf{q}} \quad (34)$$

where the spin operator $\hat{\mathbf{s}}$ appears as a whole for the five-band. At the RPA level, for example,

$$\begin{aligned} \chi_{(\text{it})}^{+-}(\mathbf{q}, \mathbf{q}, t) &= -i \langle T \hat{\mathbf{s}}_{\mathbf{q}}^+(t) \hat{\mathbf{s}}_{-\mathbf{q}}^- \rangle_0 + \frac{i}{2} \langle T \hat{\mathbf{s}}_{\mathbf{q}}^+(t) H_{J_H}(t_1) H_{J_H}(t_2) \hat{\mathbf{s}}_{-\mathbf{q}}^- \rangle_0 + O(H_{J_H}^4) \\ &= \chi_{(\text{it})0}^{+-}(\mathbf{q}, \mathbf{q}, t) + \left(\frac{J_0}{2}\right)^2 \int_{-\infty}^{\infty} dt_1 \int_{-\infty}^{\infty} dt_2 [\chi_{(\text{it})0}^{+-}(\mathbf{q}, \mathbf{q}, t-t_1) \chi_{(\text{lo})0}^{+-}(\mathbf{q}, \mathbf{q}, t_1-t_2) \chi_{(\text{it})0}^{+-}(\mathbf{q}, \mathbf{q}, t_2) \\ &\quad + \chi_{(\text{it})0}^{+-}(\mathbf{q}, \mathbf{q}, t-t_1) \chi_{(\text{lo})0}^{+-}(\mathbf{q}, \mathbf{q}, t_1-t_2) \chi_{(\text{it})0}^{+-}(\mathbf{q}+\mathbf{Q}_s, \mathbf{q}, t_2) \\ &\quad + \chi_{(\text{it})0}^{+-}(\mathbf{q}, \mathbf{q}+\mathbf{Q}_s, t-t_1) \chi_{(\text{lo})0}^{+-}(\mathbf{q}+\mathbf{Q}_s, \mathbf{q}+\mathbf{Q}_s, t_1-t_2) \chi_{(\text{it})0}^{+-}(\mathbf{q}+\mathbf{Q}_s, \mathbf{q}, t_2) \\ &\quad + \chi_{(\text{it})0}^{+-}(\mathbf{q}, \mathbf{q}+\mathbf{Q}_s, t-t_1) \chi_{(\text{lo})0}^{+-}(\mathbf{q}+\mathbf{Q}_s, \mathbf{q}, t_1-t_2) \chi_{(\text{it})0}^{+-}(\mathbf{q}, \mathbf{q}, t_2)] + \dots, \end{aligned} \quad (35)$$

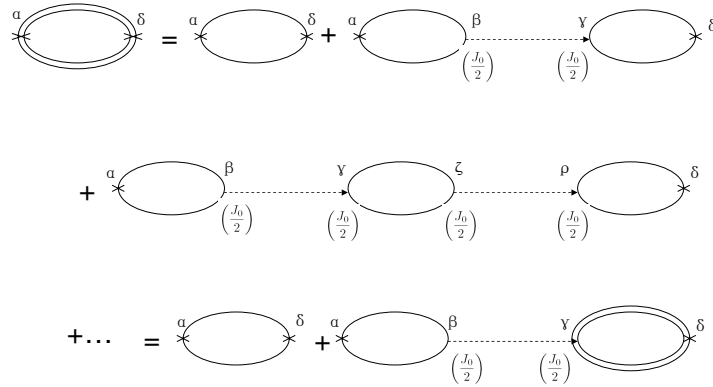


FIG. 5: (Color online) Feynman diagrams of RPA for dynamic spin correlation of itinerant electrons. Here the single line bubbles denote the dynamic spin correlation function of (free) itinerant electrons, $\hat{\chi}_{(\text{it})0}^{+-}(\mathbf{q}, \omega)$, the double line bubbles are the renormalized dynamic spin correlation function of itinerant electrons, $\hat{\chi}_{(\text{it})}^{+-}(\mathbf{q}, \omega)$, the dotted lines are the dynamic spin correlation function of local moments, $\hat{\chi}_{(\text{lo})0}^{+-}(\mathbf{q}, \omega)$. The indices α, β, \dots label the matrix elements defined in (36).

which is illustrated diagrammatically by Fig. 5.

To make the formulation more compact, we define a 2×2 matrix $\hat{\chi}^{+-}(\mathbf{q}, \omega)$ with the components

$$\begin{aligned}
 \hat{\chi}_{(1,1)}^{+-}(\mathbf{q}, \omega) &\equiv \chi^{+-}(\mathbf{q}, \mathbf{q}, \omega) \\
 \hat{\chi}_{(1,2)}^{+-}(\mathbf{q}, \omega) &\equiv \chi^{+-}(\mathbf{q}, \mathbf{q} + \mathbf{Q}_s, \omega) \\
 \hat{\chi}_{(2,2)}^{+-}(\mathbf{q}, \omega) &\equiv \chi^{+-}(\mathbf{q} + \mathbf{Q}_s, \mathbf{q} + \mathbf{Q}_s, \omega) \\
 \hat{\chi}_{(2,1)}^{+-}(\mathbf{q}, \omega) &\equiv \chi^{+-}(\mathbf{q} + \mathbf{Q}_s, \mathbf{q}, \omega).
 \end{aligned} \tag{36}$$

With this definition, the Fourier transformation of (35) reads

$$\hat{\chi}_{(\text{it})(1,1)}^{+-} = \hat{\chi}_{(\text{it})0(1,1)}^{+-} + \left(\frac{J_0}{2}\right)^2 \sum_{i,j=1,2} \hat{\chi}_{(\text{it})0(1,i)}^{+-} \hat{\chi}_{(\text{lo})0(i,j)}^{+-} \hat{\chi}_{(\text{it})0(j,1)}^{+-} + \dots, \tag{37}$$

and more generally

$$\hat{\chi}_{(\text{it})(i,j)}^{+-} = \hat{\chi}_{(\text{it})0(i,j)}^{+-} + \left(\frac{J_0}{2}\right)^2 \sum_{i',j'=1,2} \hat{\chi}_{(\text{it})0(i,i')}^{+-} \hat{\chi}_{(\text{lo})0(i',j')}^{+-} \hat{\chi}_{(\text{it})0(j',j)}^{+-} + \dots. \tag{38}$$

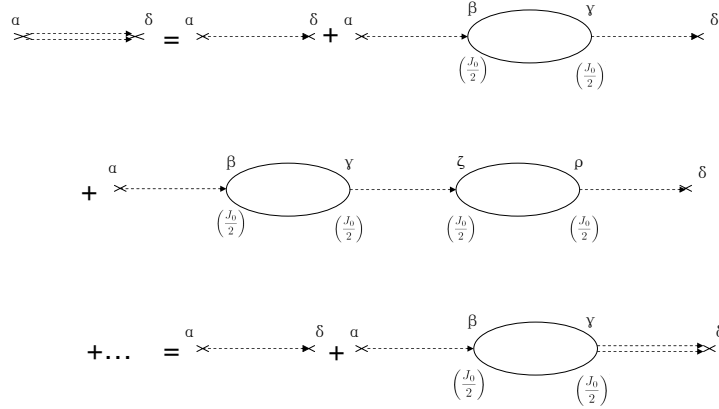


FIG. 6: (Color online) Feynman diagrams of RPA for dynamic spin correlation of local moments. Here the double dotted lines are the renormalized dynamic spin correlation function of local moments $\hat{\chi}_{(\text{lo})}^{+-}(\mathbf{q}, \omega)$. The other symbols are the same as in Fig. 5.

As the Dyson equations in a compact matrix form, the above RPA result for the itinerant electrons can be reexpressed as

$$\hat{\chi}_{(\text{it})}^{+-}(\mathbf{q}, \omega) = \left[I - \left(\frac{J_0}{2}\right)^2 \hat{\chi}_{(\text{it})0}^{+-}(\mathbf{q}, \omega) \hat{\chi}_{(\text{lo})0}^{+-}(\mathbf{q}, \omega) \right]^{-1} \hat{\chi}_{(\text{it})0}^{+-}(\mathbf{q}, \omega), \quad (39)$$

and similarly for the local moment part illustrated by Fig. 6, we have

$$\hat{\chi}_{(\text{lo})}^{+-}(\mathbf{q}, \omega) = \left[I - \left(\frac{J_0}{2}\right)^2 \hat{\chi}_{(\text{lo})0}^{+-}(\mathbf{q}, \omega) \hat{\chi}_{(\text{it})0}^{+-}(\mathbf{q}, \omega) \right]^{-1} \hat{\chi}_{(\text{lo})0}^{+-}(\mathbf{q}, \omega), \quad (40)$$

with the total dynamic spin susceptibility matrix given by

$$\hat{\chi}_{\text{RPA}}^{+-}(\mathbf{q}, \omega) = \hat{\chi}_{(\text{it})}^{+-}(\mathbf{q}, \omega) + \hat{\chi}_{(\text{lo})}^{+-}(\mathbf{q}, \omega). \quad (41)$$

B. Collective spin modes

Now we focus on the total dynamic spin susceptibility defined by

$$\chi''_{\text{RPA}}(\mathbf{q}, \omega) = -2\text{Im}\hat{\chi}_{\text{RPA}(1,1)}^{+-}(\mathbf{q}, \omega) \quad (42)$$

which can be numerically determined based on the RPA expressions (39), (40) and (41) given in the above subsection.

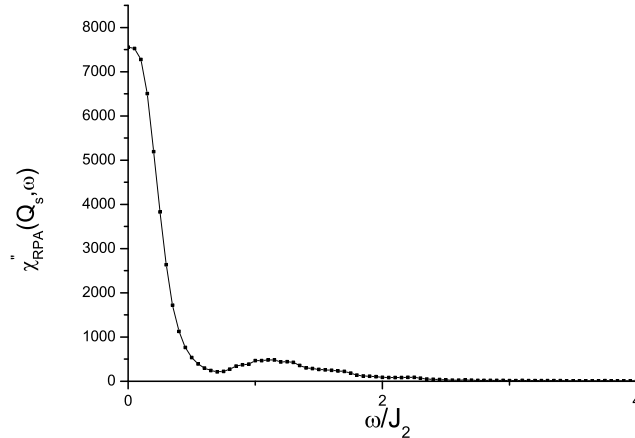


FIG. 7: (Color online) Total dynamic spin-susceptibility of coupled system in RPA level $\chi''_{\text{RPA}}(\mathbf{q}, \omega)$ fixing $\mathbf{q} = \mathbf{Q}_s$.

In Fig. 7, $\chi''_{\text{RPA}}(\mathbf{q}, \omega)$ at a fixing $\mathbf{q} = \mathbf{Q}_s$ is shown as a function of ω . Here we find a sharp peak emerges at $\omega = 0$, in contrast to Figs. 3 and 4. Namely a zero-mode (Goldstone mode) pole is indeed restored at $\mathbf{q} = \mathbf{Q}_s$ in the RPA spin-spin correlation function. Mathematically, it originates from the vanishing denominator in (39) and (40).

It is interesting to note that besides the Goldstone mode, there remains a high-energy mode as represented by the hump in Fig. 7. It can be traced to the pole of $\hat{\chi}_{(10)0}^{+-}(\mathbf{q}, \omega)$ (cf. Fig. 3), only broadened through the scattering with the itinerant electrons. In other words, the gapped collective mode of the local moments identified in the mean-field state in the previous section is still present at the RPA level. Physically this gapped mode is an “out of phase” fluctuations of the local moments relative to the magnetization of itinerant electrons, while the Goldstone mode is the “in phase” fluctuations of the locked magnetizations from the local moments and itinerant electrons.

To display the spin dynamics of the system in the whole BZ, the calculated $\chi''_{\text{RPA}}(\mathbf{q}, \omega)$ is presented in Fig. 8(a) with the x -axis representing the momentum \mathbf{q} along the high-symmetry lines in the reduced BZ and the y -axis for the frequency ω , while the brightness depicting the spectral weight $\chi''_{\text{RPA}}(\mathbf{q}, \omega)$. From Fig. 8(a), it is clearly shown that the spin excitation spectrum in the AF ordered phase is separated into two branches, i.e. the lower Goldstone-mode branch and the upper “out-of-phase” mode branch. The dispersions of the two modes are illustrated in Fig. 8(b), which are defined by (\mathbf{q}, ω) at the largest (brightest)

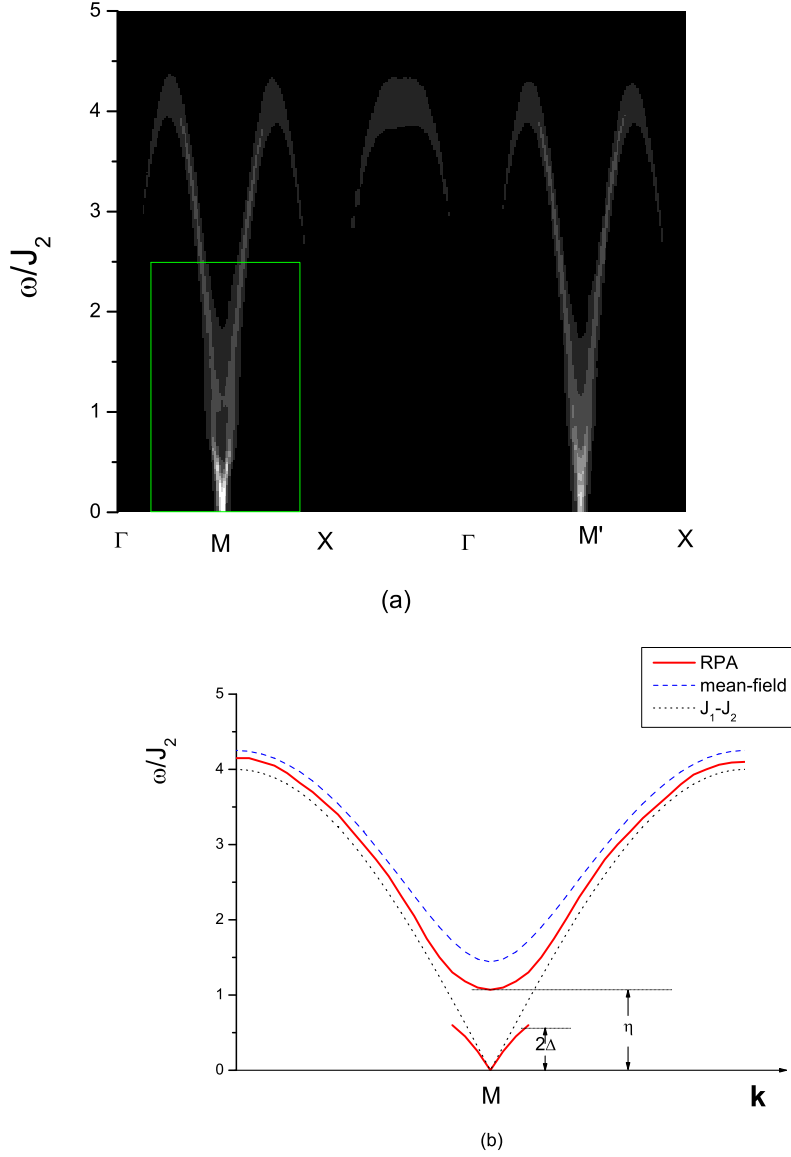


FIG. 8: (Color online) (a) The brightness represents the spectral weight of the dynamic spin susceptibility χ''_{RPA} in the \mathbf{q} and ω space. (b) The dispersions of two branches of the collective spin mode as read from (a). The dispersions of the spin-wave of the pure $J_1 - J_2$ model (dotted) and that with a gap opening at the mean-field level (dashed) are also shown for comparison.

$\chi''_{\text{RPA}}(\mathbf{q}, \omega)$ in Fig. 8(a). The spin wave dispersion of the pure $J_1 - J_2$ model, i.e., (16) and that of the gapped one, (18), due to coupling to the SDW order of the itinerant electrons are also shown for comparison.

The lower branch Goldstone mode in Fig. 8(b) is well-defined within a small region

which centers at the AF wavevector \mathbf{Q}_s , upper-bounded by the SDW gap, i.e. $2\Delta_{\text{SDW}}$ of the itinerant electrons, beyond which it decays quickly due to the scattering with the particle-hole continuum of itinerant electrons (cf. Fig. 4). Inside the SDW order gap, such a Goldstone mode is protected and is decoupled from the itinerant electrons due to the reconstruction of the Fermi surface shown in Figs. 1 and 2.

On the other hand, the high energy “out-of-phase” mode is mainly contributed by the local moments and present throughout the BZ. It gets slight renormalization and broadening due to the scattering from the itinerant electrons at the RPA level, but more or less follows the dispersion obtained in the mean-field treatment (dotted), with a gap η

$$\eta \approx \omega_{\mathbf{Q}_s}. \quad (43)$$

It is noted that the Goldstone mode will be fragile against the ion-anisotropy. By adding an ion-anisotropy term,

$$H_{(\text{ion})} = -J_z \sum_i (S_i^z)^2 \quad (44)$$

the spin-rotational symmetry will be broken in H_{lo} . By using the spin-wave expansion

$$H_{(\text{ion})} = 2SJ_z \sum_k' (a_{\mathbf{k}}^\dagger a_{\mathbf{k}} + b_{\mathbf{k}}^\dagger b_{\mathbf{k}}) + \text{const.} \quad (45)$$

one finds the spin-excitation spectrum (16) acquires an ion-anisotropy gap

$$\omega_{\mathbf{k}} = S\sqrt{(\Gamma_{\mathbf{k}} + 2J_z)^2 - M_{\mathbf{k}}^2}. \quad (46)$$

At the RPA level, the Goldstone spin wave will also become gapped and its spectrum weight is reduced with reference to that without ion-anisotropy, as clearly shown in Fig. 9. When one further increases J_z , the Goldstone mode disappears, but the gapped “out-of-phase” collective mode remains robust and insensitive to the ion-anisotropy.

Therefore, in the present coupled local moment and itinerant electron system, the Goldstone theorem still holds for a spontaneously symmetry breaking state with AF ordering at the RPA level. However, the Goldstone mode is very sensitive to the presence of ion-anisotropy and does not play an important role for charge dynamics as it is decoupled from the itinerant electrons. On the other hand, the gapped “out-of-phase” collective mode is more prominent which extends over the whole BZ with a spin-wave bandwidth $\sim 4J_2$ and can be easily probed by neutron scattering experiments. Such two-branch collective spin

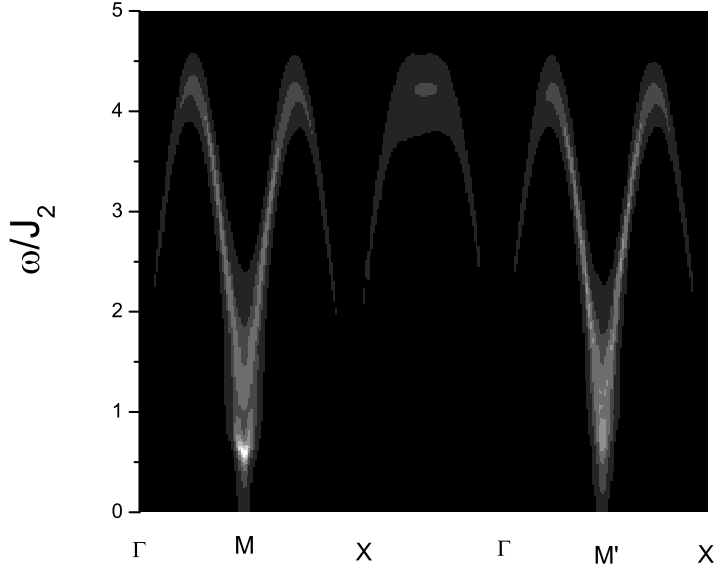


FIG. 9: (Color online) The dynamic spin susceptibility similar to Fig. 8, but with an additional ion-anisotropy $J_z = 1$ meV.

excitations are unique prediction for the AF ordered phase. In the next section, the charge response will be further examined based on the scattering of such collective spin modes with the itinerant electrons in SDW ordering.

IV. CHARGE DYNAMICS

In this section, we study the charge dynamics in the coupled local-moment and itinerant-electron system in the AF ordered phase. Here the itinerant electrons in the Fermi surface region will be highly coherent even in the presence of the gapless Goldstone mode.

A. Self-energy of itinerant electrons

By going beyond the mean-field linearization in (5), we shall consider the scattering based on

$$\begin{aligned}
H_{J_H} &\rightarrow H'_I = -\frac{J_0}{2\sqrt{N}} \sum_{\mathbf{k} \in R, \mathbf{q} \in R, \alpha\beta} c_{\mathbf{k}\alpha\downarrow}^\dagger c_{\mathbf{q}\beta\uparrow} \left[S_{\mathbf{q}-\mathbf{k}}^+ V_{\mathbf{k},\mathbf{q}}^{(1)}(\alpha, \beta) + S_{\mathbf{q}-\mathbf{k}+\mathbf{Q}_s}^+ V_{\mathbf{k},\mathbf{q}}^{(2)}(\alpha, \beta) \right] + h.c. \\
&\equiv -\frac{J_0}{2\sqrt{N}} \sum_{\mathbf{k} \in R, \mathbf{q} \in R, \alpha\beta} c_{\mathbf{k}\alpha\downarrow}^\dagger c_{\mathbf{q}\beta\uparrow} R_{\mathbf{k}\mathbf{q}\alpha\beta}^+ + h.c.
\end{aligned} \tag{47}$$

where the $V_{\mathbf{k},\mathbf{q}}^{(1,2)}(\alpha, \beta)$ are defined by (32). Here we retain only the scattering of itinerant electrons with the transverse fluctuations of local moments as the longitudinal fluctuations in S^z are gapped with $\langle S^z \rangle \neq 0$.

The single-particle Green's Function can be evaluated perturbatively by

$$G_{\alpha\beta\downarrow}(\mathbf{k}, \omega) = G_{\alpha\beta\downarrow}^0(\mathbf{k}, \omega) + \sum_{\gamma\epsilon} G_{\alpha\gamma\downarrow}^0(\mathbf{k}, \omega) \Sigma_{\gamma\epsilon\downarrow}(\mathbf{k}, \omega) G_{\epsilon\beta\downarrow}^0(\mathbf{k}, \omega) + O(H_I^4), \tag{48}$$

where the self-energy

$$\Sigma_{\gamma\epsilon\downarrow}(\mathbf{k}, \omega) = \frac{iJ_0^2}{4N} \sum_{\mathbf{q} \in R, \theta\xi} \int_{-\infty}^{+\infty} \frac{d\Omega}{2\pi} G_{\theta\xi\uparrow}^0(\mathbf{q}, \omega - \Omega) \chi_{(R)\mathbf{k}\mathbf{q}\gamma\theta\xi\epsilon}^{+-}(\Omega), \tag{49}$$

with

$$\begin{aligned}
\chi_{(R)\mathbf{k}\mathbf{q}\gamma\theta\xi\epsilon}^{+-}(\Omega) &= \hat{\chi}_{(lo)(1,1)}^{+-}(\mathbf{q} - \mathbf{k}, \Omega) |V^{(1)}|^2 + \hat{\chi}_{(lo)(1,2)}^{+-}(\mathbf{q} - \mathbf{k}, \Omega) V^{(1)} V^{(2)*} + \\
&\quad \hat{\chi}_{(lo)(2,1)}^{+-}(\mathbf{q} - \mathbf{k}, \Omega) V^{(2)} V^{(1)*} + \hat{\chi}_{(lo)(2,2)}^{+-}(\mathbf{q} - \mathbf{k}, \Omega) |V^{(2)}|^2.
\end{aligned} \tag{50}$$

Here the matrix $\hat{\chi}_{(lo)}^{+-}$ is the dynamic spin correlation function for the local-moment in the RPA level defined in (40). Fig. 10 and Fig. 11 show the corresponding Feynman diagrams of the self-energy correction for itinerant electrons.

The equation (48) can be further expressed in a 10×10 matrix formalism by

$$\begin{aligned}
G_{\mathbf{k},\omega} &= G_{\mathbf{k},\omega}^0 + G_{\mathbf{k},\omega}^0 \Sigma_{\mathbf{k},\omega} G_{\mathbf{k},\omega}^0 + \dots \\
&= G_{\mathbf{k},\omega}^0 + G_{\mathbf{k},\omega}^0 \Sigma_{\mathbf{k},\omega} G_{\mathbf{k},\omega}
\end{aligned} \tag{51}$$

which gives rise to $G_{\mathbf{k},\omega} = \left((G_{\mathbf{k},\omega}^0)^{-1} - (\Sigma_{\mathbf{k},\omega}) \right)^{-1}$. Here we have omitted the spin index as they are in fact spin-independent.

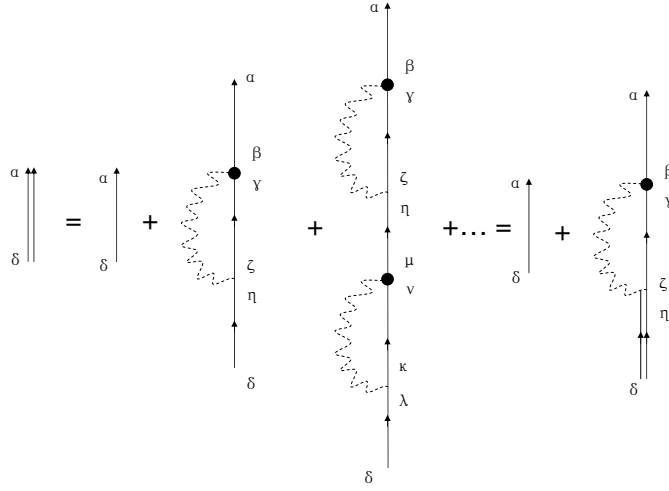


FIG. 10: (Color online) Feynman diagrams of self-energy correction for itinerant-electrons. Here the single black lines denote the propagators of (free) itinerant-electrons, $G_{\alpha\delta}^0(\mathbf{k}, \omega)$, the double black lines are the renormalized propagators of itinerant-electrons, $G_{\alpha\delta}(\mathbf{k}, \omega)$, the dotted wavy lines are the modified dynamic spin correlation of local-moments in the RPA level $\chi_{(R)\mathbf{k}\mathbf{q}\gamma\theta\xi\epsilon}^{+-}(\Omega)$ defined by (50). The indices $\alpha, \beta, \gamma, \rho, \varsigma$, label different bands.

By noting that the zero-th order single-particle Green's function is diagonal, through the Lehmann representation we have for $\omega > 0$

$$-\text{Im}\Sigma_{\gamma\epsilon}(\mathbf{k}, \omega) = \frac{J_0^2}{4N} \sum_{\mathbf{q} \in R, \theta} \int_{-\infty}^{+\infty} \frac{d\Omega}{4\pi} \rho_{\theta}^0(\mathbf{q}, \omega - \Omega) D_{\gamma\theta\epsilon}^{+-}(\mathbf{k} - \mathbf{q}, \Omega) [n_B(\Omega) + n_F(\Omega - \omega)], \quad (52)$$

where

$$\rho_{\theta}^0(\mathbf{q}, \omega) \equiv -2\text{Im}G_{\theta\theta}^0(\mathbf{q}, \omega) \quad (53)$$

and

$$D_{\gamma\theta\epsilon}^{+-}(\mathbf{k} - \mathbf{q}, \Omega) \equiv -2\text{Im}\chi_{(R)\mathbf{k}\mathbf{q}\gamma\theta\theta\epsilon}^{+-}(\Omega), \quad (54)$$

are the spectral functions of single-particle and the modified dynamic spin susceptibility of the local-moment, respectively.

At zero temperature, the imaginary self-energy (52) can be further evaluated as (for $\omega > 0$)

$$-\text{Im}\Sigma_{\alpha\beta}(\mathbf{k}, \omega) = \frac{J_0^2}{8N} \sum_{\mathbf{q} \in R, \theta, 0 < E_{\mathbf{q}\theta} < \omega} D_{\alpha\theta\beta}^{+-}(\mathbf{k} - \mathbf{q}, \omega - E_{\mathbf{q}\theta}). \quad (55)$$

$$\Sigma_{\gamma\epsilon\downarrow}(\vec{k}, \omega) = \chi_{(R)\vec{k}\vec{q}\gamma\theta\xi\epsilon}^{+-}(\Omega) G_{\theta\xi\downarrow}^0(\vec{q}, \omega - \Omega)$$

FIG. 11: (Color online) Self-energy correction for itinerant-electrons

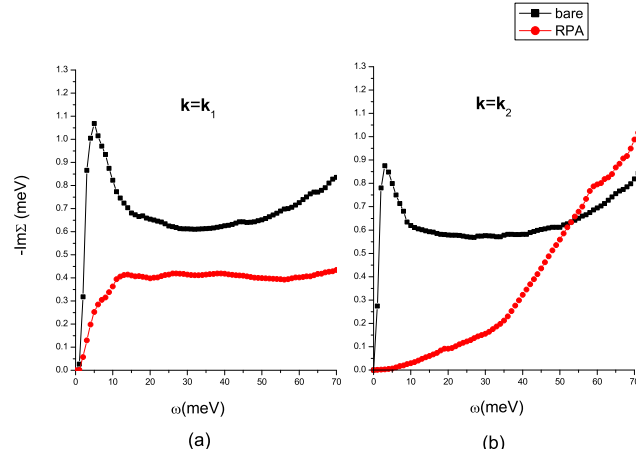


FIG. 12: (Color online) The imaginary part of the quasiparticle self-energy $-\text{Im}\Sigma_{\alpha\alpha}(\mathbf{k}, \omega)$ at two typical \mathbf{k} -points marked in Fig. 2(a) is shown. The red-circled curve is for incorporating the scattering with the full collective mode at the RPA level and the black-squared one is for the scattering with the bare local moment fluctuations governed by H_{10} .

In Fig. 12, the $-\text{Im}\Sigma_{\alpha\alpha}(\mathbf{k}, \omega)$ as a function of ω is shown at two typical momenta, (\mathbf{k}_1, α_1) and (\mathbf{k}_2, α_2) , respectively, which are marked at Fermi pockets in Fig. 2(a). It shows that the life time of the quasiparticle excitations at these points of Fermi pockets actually gets substantially *enhanced* at low ω in the collinear AF ordered state (solid circles), as compared

to an artificial case (solid squares) without an induced SDW order appearing in itinerant electrons such that there is no gap η opened up in the “out-of-phase” mode. It implies that although in the normal state the itinerant electrons may be strongly scattered by the low-lying local moment fluctuations, the sharp coherence of quasiparticles will emerge in the AF state, where the gapless Goldstone mode is essentially decoupled from the particle-hole continuum and the “out-of-phase” mode is gapped.

B. Optical conductivity

Finally, let us examine the overall structure of the optical conductivity $\sigma(\omega)$ at the mean-field and RPA levels. It is related to the current-current correlation function $G_J(\omega)$ through the relation

$$\sigma(\omega) = -\frac{1}{\omega} \text{Im} G_J(\omega), \quad (56)$$

where $G_J(\omega)$ is the Fourier transformation of the current-current correlator

$$G_J(t) \equiv -i \langle T J(t) J(0) \rangle. \quad (57)$$

Here J denotes the $\mathbf{q} = 0$ current operator \mathbf{J} along, say, the x axis for the five-band model (2) defined by

$$\begin{aligned} \mathbf{J} &= \left. \frac{\partial H_{it}(\mathbf{A})}{\partial \mathbf{A}} \right|_{\mathbf{A}=0} \\ &= \sum_{\mathbf{k}\sigma mn} \vec{\nabla}_{\mathbf{k}} f_{mn}(\mathbf{k}) c_{\mathbf{k}m\sigma}^{\dagger} c_{\mathbf{k}n\sigma} \\ &= \sum_{\mathbf{k} \in R, \sigma mn\alpha\beta} c_{\mathbf{k}\alpha\sigma}^{\dagger} c_{\mathbf{k}\beta\sigma} \left[\vec{\nabla}_{\mathbf{k}} f_{mn}(\mathbf{k}) U_{\mathbf{k}\sigma}^*(m, \alpha) U_{\mathbf{k}\sigma}(n, \beta) + \vec{\nabla}_{\mathbf{k}} f_{mn}(\mathbf{k} + \mathbf{Q}_s) U_{\mathbf{k}\sigma}^*(m + 5, \alpha) U_{\mathbf{k}\sigma}(n + 5, \beta) \right] \\ &\equiv \sum_{\mathbf{k} \in R, \sigma\alpha\beta} V_{\mathbf{k}\sigma\alpha\beta} c_{\mathbf{k}\alpha\sigma}^{\dagger} c_{\mathbf{k}\beta\sigma}. \end{aligned} \quad (58)$$

Omitting the vertex-correction, we find

$$G_J(\omega) = -\frac{i}{N} \sum_{\mathbf{k} \in R, \sigma, \alpha\beta, \alpha'\beta'} \int_{-\infty}^{+\infty} \frac{d\Omega}{2\pi} V_{\mathbf{k}\sigma\alpha\beta} V_{\mathbf{k}\sigma\alpha'\beta'} G_{\beta'\alpha\sigma}(\mathbf{k}, \Omega) G_{\beta\alpha'\sigma}(\mathbf{k}, \Omega + \omega). \quad (59)$$

with the Feynman diagrams shown in Fig. 13. Denoting

$$\rho_{\alpha\beta}(\mathbf{k}, \omega) \equiv -2 \text{Im} G_{\alpha\beta\sigma}(\mathbf{k}, \omega) \text{sgn}(\omega), \quad (60)$$

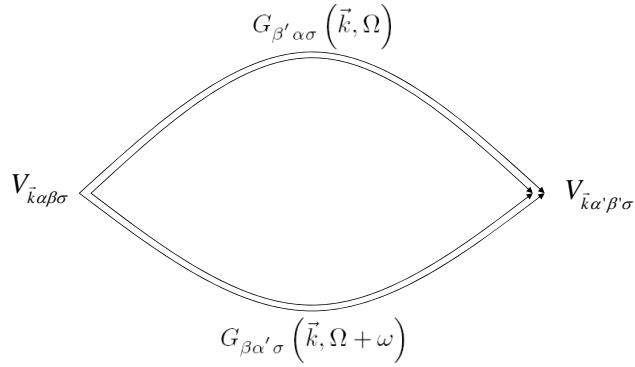


FIG. 13: (Color online) Current-current correlation function for itinerant-electrons. Here the double black lines are the renormalized proporgators of itinerant-electrons.

at $T = 0$ we obtain

$$-\text{Im}G_J = \frac{1}{N} \sum_{\mathbf{k} \in R, \sigma, \alpha\beta, \alpha'\beta'} \int_{-\omega}^0 \frac{d\Omega}{2\pi} V_{\mathbf{k}\sigma\alpha\beta} V_{\mathbf{k}\sigma\alpha'\beta'} \rho_{\beta'\alpha}(\mathbf{k}, \Omega) \rho_{\beta\alpha'}(\mathbf{k}, \Omega + \omega). \quad (61)$$

such that

$$\sigma(\omega) = \frac{1}{N\omega} \sum_{\mathbf{k} \in R, \sigma, \alpha\beta, \alpha'\beta'} \int_{-\omega}^0 \frac{d\Omega}{2\pi} V_{\mathbf{k}\sigma\alpha\beta} V_{\mathbf{k}\sigma\alpha'\beta'} \rho_{\beta'\alpha}(\mathbf{k}, \Omega) \rho_{\beta\alpha'}(\mathbf{k}, \Omega + \omega). \quad (62)$$

The calculated optical conductivity $\sigma(\omega)$ is shown in Fig. 14. The black-squared curve shows the result for the bare five-band itinerant electrons and the red circles represent the result of the SDW reconstructed bands. Note that the multi-peak structure is mainly due to the multi-band effect with the lower ones change significantly in the SDW state. Furthermore, by incorporating the scattering with the collective spin modes at the RPA level, as shown by the blue triangles in Fig. 14, no significant change has been found in the optical conductivity with $\mathbf{q} = 0$. It clearly illustrated that the itinerant electrons remain very coherent in the AF ordered phase, where the low-lying Goldstone mode does not strongly scatter the quasiparticles as expected.

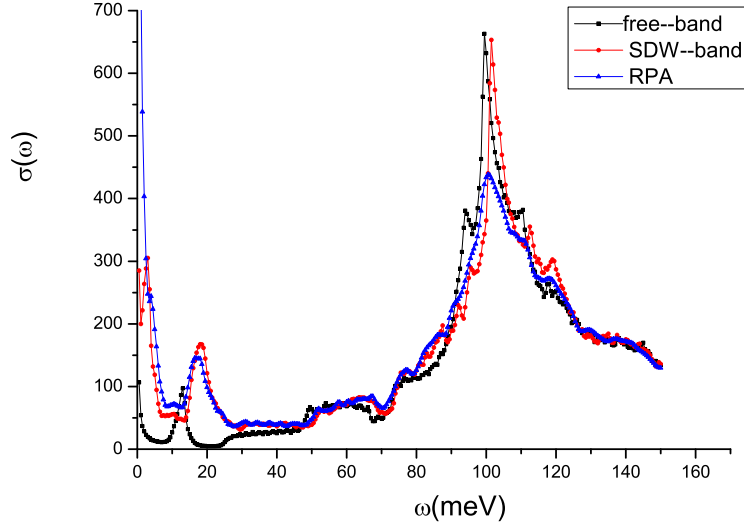


FIG. 14: (Color online) The optical conductivity $\sigma(\omega)$ in the AF ordered state (blue solid triangle) which shows that the quasiparticles remain quite coherent as compared to the case without incorporating the scattering with the collective spin modes (red solid circles). For comparison, $\sigma(\omega)$ for the pure five-band model without the SDW reconstruction is shown (black square).

V. DISCUSSION AND CONCLUSION

In this work, we have studied the collective spin excitations in the AF ordered phase of a multi-component system composed of coexistent itinerant and localized electrons. The main prediction is that a usual spin mode is split into two branches in such a multi-band system with orbital-selective Mott transition. The lower branch is a gapless Goldstone mode which is recovered at the RPA level and is quickly damped above $2\Delta_{\text{SDW}}$ by coupling to the particle-hole continuum of itinerant electrons, similar to the case in which the SDW order is due to the pure Fermi-surface nesting effect for itinerant electrons. However, an upper branch remnant spin wave reemerges above the SDW gap over a much wider energy $\sim J_2$ which is dominantly contributed by the local moment fluctuations. Here the lower and upper branches can be regarded as in-phase and out-of-phase combinations of the spin fluctuations from the itinerant and Mott-localized electrons, which are clearly distinguished from the single mode in a conventional AF state either due to the pure Fermi-surface nesting effect for itinerant electrons or AF superexchanges of local moments.

Experimentally the high-energy spin-wave excitation has been clearly observed by the neutron scattering experiments over an energy scale $\sim J_2$ and presumably survives in the high-temperature regime above the ordered phase. However, a small gap ($\sim 6 - 10$ meV) has been generally found in SrFe_2As_2 and BaFe_2As_2 , and interpreted as due to ion-anisotropy^{28,29}. As shown in this work, a small ion-anisotropy can indeed easily destroy the lower branch Goldstone mode, while the upper branch is more robust. It remains to be seen if the lower branch spin mode can be unambiguously identified for a sample with less ion-anisotropy.

Another distinct property of the present system is that the itinerant electrons become very coherent in the AF ordered phase, leading to a good metallic behavior after the AF transition. This is in contrast to the presumably strong scattering between the itinerant electrons and local moments in the normal state, where due to the very fact that the momentum displacement of the hole-electron Fermi pockets of the itinerant electrons matches with the AF wavevector of the local moments, there exists a strongly enhanced interaction, i.e., the “*resonant effect*” around \mathbf{Q}_s , between the two subsystems. It provides the strong scattering source responsible for a drastic change in the charge response once the system enters the AF long-range ordered state at low-temperature. By forming a joint magnetic ordering, the two subsystem effectively get “decoupled” as the AF fluctuations of the local moments gain a gap η as the out-of-phase collective mode. On the other hand, the gapless Goldstone mode is effectively decoupled from the itinerant electrons in the long-wavelength, thanks to the Fermi surface reconstruction by the SDW order.

Therefore, the collective fluctuations of the local moments can serve as the main driving force for both the AF ordering as well as the superconducting pairing in the system via the “resonant effect” on itinerant electrons, as first pointed out in Ref.²⁵. The resulting magnetic and charge properties in the AF ordered state, in particular the two branch collective spin modes predicted in the present work, can be further tested by experiment in order to establish the relevance of the model with the iron pnictides.

Acknowledgments

We acknowledge stimulating discussions with X.H. Chen, P.C. Dai, D.L. Feng, D.H. Lee, P.A. Lee, T. Li, Z.Y. Lu, N.L. Wang, T. Xiang, Y.Z. You, G.M. Zhang and H. Yao.

The authors are grateful for the partial support by NSFC grant Nos. 10688401, 10704008, 10834003 and 10874017 as well as the National Program for Basic Research of MOST.

* Electronic address: weng@tsinghua.edu.cn

- ¹ Y. Kamihara, T. Watanabe, M. Hirano, and H. Hosono, *J. Am. Chem. Soc.* 130, 3296 (2008).
- ² P. W. Anderson, *Science* 235, 1196 (1987).
- ³ J. Dong, H. J. Zhang, G. Xu, Z. Li, G. Li, W. Z. Hu, D. Wu, G. F. Chen, X. Dai, J. L. Luo, Z. Fang, and N. L. Wang, *Europhys. Lett.* 83, 27006 (2008).
- ⁴ C. Cao, P. J. Hirschfeld, and H. P. Cheng, *Phys. Rev. B* 77, 220506 (R) (2008)
- ⁵ D. J. Singh and M. H. Du, *Phys. Rev. Lett.* 100, 237003 (2008)
- ⁶ I. I. Mazin, D. J. Singh, M. D. Johannes and M. H. Du, *Phys. Rev. Lett.* 101, 057003 (2008).
- ⁷ K. Kuroki, S. Onari, R. Arita, H. Usui, Y. Tanaka, H. Kontani, and H. Aoki, *Phys. Rev. Lett.* 101, 087004 (2008)
- ⁸ C. de la Cruz, Q. Huang, J. W. Lynn, J. Li, W. Ratcliff II, J. L. Zarestky, H. A. Mook, G. F. Chen, J. L. Luo, N. L. Wang, and Pengcheng Dai, *Nature (London)* 453, 899 (2008)
- ⁹ D. H. Lu, M. Yi, S. K. Mo, A. S. Erickson, J. Analytis, J. H. Chu, D. J. Singh, Z. Hussain, T. H. Geballe, I. R. Fisher, Z. X. Shen, *Nature (London)* 455, 81-84 (4 September 2008)
- ¹⁰ G. Liu, H. Liu, L. Zhao, W. Zhang, X. Jia, J. Meng, X. Dong, G. F. Chen, G. Wang, Y. Zhou, Y. Zhu, X. Wang, Z. Xu, C. Chen and X. J. Zhou, *Phys. Rev. B* 80, 134519 (2009).
- ¹¹ L. X. Yang, Y. Zhang, H. W. Ou, J. F. Zhao, D. W. Shen, B. Zhou, J. Wei, F. Chen, M. Xu, C. He, Y. Chen, Z. D. Wang, X. F. Wang, T. Wu, G. Wu, X. H. Chen, M. Arita, K. Shimada, M. Taniguchi, Z. Y. Lu, T. Xiang, D. L. Feng, *Phys. Rev. Lett.* 102, 107002 (2009).
- ¹² M. Tropeano, arXiv:0809.3500.
- ¹³ W. Z. Hu, G. Li, P. Zheng, G. F. Chen, J. L. Luo, and N. L. Wang, *Phys. Rev. Lett.* 101, 257005 (2008).
- ¹⁴ T. Yildirim, *Phys. Rev. Lett.* 101, 057010 (2008).
- ¹⁵ Q. Si and E. Abrahams, *Phys. Rev. Lett.* 101, 076401 (2008).
- ¹⁶ F. Ma, Z. Y. Lu, T. Xiang, *Phys. Rev. B* 78, 224517 (2008).
- ¹⁷ J. Zhao, D. T. Adroja, D. X. Yao, R. Bewley, S. Li, X. F. Wang, G. Wu, X. H. Chen, J. P. Hu, and P. C. Dai, *Nature Physics* 5, 555 (2009).

- ¹⁸ X. F. Wang, T. Wu, G. Wu, H. Chen, Y. L. Xie, J. J. Ying, Y. J. Yan, R. H. Liu and X. H. Chen, *Phys. Rev. Lett.* 102, 117005(2009).
- ¹⁹ R. Klingeler, N. Leps, I. Hellmann, A. Popa, U. Stockert, C. Hess, V. Kataev, H. J. Grafe, F. Hammerath, G. Lang, G. Behr, L. arnagea, S. Singh, and B. Buchner, *Phys. Rev. B* 81, 024506 (2010).
- ²⁰ G.M. Zhang, Y.H. Su, Z.Y. Lu, Z.Y. Weng, D.H. Lee, and T. Xiang, *Europhys. Lett.* 86, 37006 (2009).
- ²¹ X. H. Chen, T. Wu, G. Wu, R. H. Liu, H. Chen, D. F. Fang, *Nature* 453,761-762(2008).
- ²² Y. Luo, Y. Li, S. Jiang, J. Dai, G. Cao, Z. Xu, arXiv:0907.2961
- ²³ T. Sato, K. Nakayama, Y. Sekiba, P. Richard, Y.-M. Xu, S. Souma, T. Takahashi, G. F. Chen, J. L. Luo, N. L. Wang, and H. Ding, *Phys. Rev. Lett.* 103 (2009) 047002;
- ²⁴ C. Liu, G. D. Samolyuk, Y. Lee, N. Ni, T. Kondo, A. F. Santander-Syro, S. L. Bud'ko, J. L. McChesney, E. Rotenberg, T. Valla, A. V. Fedorov, P. C. Canfield, B. N. Harmon, and A. Kaminski, *Phys. Rev. Lett.* 101, 177005 (2008).
- ²⁵ S. P. Kou, T. Li, Z. Y. Weng, *Europhys. Lett.* 88, 17010 (2009).
- ²⁶ L. de' Medici, S.R. Hassan, M. Capone, *J. Supercond. Nov. Magn.* 22, 535 (2009).
- ²⁷ H. Lee, Y. Z. Zhang, H. O. Jeschke, R. Valenti, arXiv:0912.4024
- ²⁸ J. Zhao,D.-X. Yao, S. Li, T. Hong, Y. Chen, S. Chang, W. Ratcliff, J. W. Lynn, H. A. Mook, G. F. Chen, J. L. Luo, N. L. Wang, E. W. Carlson, J. Hu, and P. Dai, *Phys. Rev. Lett.* 101, 167203 (2008).
- ²⁹ K. Matan, R. Morinaga, K. Iida¹, and T. J. Sato, *Phys. Rev. B* 79, 054526 (2009).